Available online at www.sciencedirect.com
ScienceDirect
International Journal of Solids and Structures 45 (2008) 3088–3106
INTERNATIONAL JOURNAL OF SOLIDS AND STRUCTURES
www.elsevier.com/locate/ijsolstr

A modified Drucker-Prager Cap model for die compaction simulation of pharmaceutical powders

L.H. Han [a,*], J.A. Elliott [a,*], A.C. Bentham [b], A. Mills [b], G.E. Amidon [c], B.C. Hancock [d]

[a] *Pfizer Institute for Pharmaceutical Materials Science, Department of Materials Science and Metallurgy, University of Cambridge, Pembroke Street, Cambridge, CB2 3QZ, UK*
[b] *Pfizer Global Research and Development, Sandwich, CT13 9NJ, UK*
[c] *University of Michigan, College of Pharmacy, 428 Church Street, Ann Arbor, MI 48109-1065, USA*
[d] *Pfizer Global Research and Development, Groton, CT 06340, USA*

Received 3 September 2007; received in revised form 19 December 2007
Available online 1 February 2008

Abstract

In this paper, we present a modified density-dependent Drucker-Prager Cap (DPC) model to simulate the compaction behaviour of pharmaceutical powders. In particular, a nonlinear elasticity law is proposed to describe the observed nonlinear unloading behaviour following compaction. To extract the material parameters for the modified DPC model, a novel experimental calibration procedure is used, based on uniaxial single-ended compaction tests using an instrumented cylindrical die. The model is implemented in ABAQUS by writing a user subroutine, and a calibration process on microcrystalline cellulose (MCC) Avicel PH101 powders is detailed. The calibrated parameters are used for the manufacturing process simulation of two kinds of typical pharmaceutical tablets: the flat-face tablet and the concave tablet with single or double radius curvatures. The model developed can describe not only the compression and decompression phases, but also the ejection phase. The model is validated by comparing finite element simulations with experimental loading–unloading curves during the manufacture of 8 and 11 mm round tablets with flat-face (FF), single radius concave (SRC) and double radius concave (DRC) profiles. Moreover, the density and stress distributions during tabletting are used to analyse and explain the failure mechanism of tablets. The results show that the proposed model can quantitatively reproduce the compaction behaviour of pharmaceutical powders and can be used to obtain the stress and density distributions during compression, decompression and ejection.

Keywords: Constitutive law; Powder compaction; Granular media; Finite element; Material parameter identification

* Corresponding authors. Tel.: +44 1223 767059; fax: +44 1223 334366.
E-mail addresses: lhh24@cam.ac.uk (L.H. Han), jae1001@cam.ac.uk (J.A. Elliott).

0020-7683/$ - see front matter © 2008 Elsevier Ltd. All rights reserved.
doi:10.1016/j.ijsolstr.2008.01.024

1. Introduction

As the most widely used dosage form for drug delivery in the pharmaceutical industry, tablets have many advantages over other dosage forms, such as low cost, long term storage stability, good tolerance to temperature and humidity and ease of use by the patient. However, some common defects, such as sticking, picking, capping and lamination, can occur during tabletting by uniaxial die compaction. Although several simple theories have been used to explain the causes of failure (Burlinson, 1968; Long, 1960), more detailed simulation and analysis of the tabletting process are imperative in order to quantitatively predict the occurrence of tablet failure and how it may manifest. Moreover, simulation of the tabletting process can also help to understand the influence of tooling properties, lubrication and compaction kinematics (e.g. compaction speed and compaction sequences), and provide the guidance for the optimisation of tooling design and the improvement of the powder formulation.

The computational modelling of powder compaction has typically been carried out by two different approaches: the discrete model method and the continuum model method. The discrete model method (Fleck, 1995; Fleck et al., 1992; Helle et al., 1985) treated each powder particle individually and analysed the contact interaction and deformation of particles, while the continuum model method considered the powder as a continuous media. Whereas the discrete model method (DiMaggio and Sandler, 1971; Khoei and Azizi, 2005; Schofield and Wroth, 1968; Shima and Oyane, 1976) was more useful for understanding the physical processes of powder compaction, the continuum model method was more suitable for engineering applications. Although a pharmaceutical powder is clearly discontinuous at the particle level, this becomes irrelevant at a larger scale of aggregation such as when it is compacted into a relatively dense compact in a die during tabletting. Therefore, the compaction behaviour of pharmaceutical powders can be studied using the principles of continuum mechanics at a macroscopic level, i.e. phenomenological models. The phenomenological models, such as critical state models like Cam-Clay plasticity models and Cap plasticity models, which were originally developed for geological materials in soil mechanics, turned out to be well suited for modelling powder compaction, especially in powder metallurgy (Aydin et al., 1997, 1996; Chtourou et al., 2002; Coube and Riedel, 2000; PM-Modnet-Modelling-Group, 1999). More recently, Drucker-Prager Cap plasticity models have been used for the analysis of compaction of pharmaceutical powders, because they can represent the densification and hardening of the powder, as well as the interparticle friction (Cunningham et al., 2004; Frenning, 2007; Michrafy et al., 2004, 2002; Sinka et al., 2003, 2004; Wu et al., 2005, 2008). However, in these studies, the Young's modulus and Poisson's ratio were assumed to be constant, which was not suitable to describe the observed nonlinear unloading behaviour of pharmaceutical powders and understand the elastic recovery of compacts during unloading and ejection. This is particularly important for tablet fracture, since the elastic recovery may initiate the cracks within compacts and produce catastrophic flaws, causing the compaction failures such as capping, lamination and chipping (Martin et al., 2003; Train, 1957). Moreover, the unsuitable material parameter identification for Drucker-Prager Cap models may result in an unrealistic simulation of the decompression phase of compaction, where the plastic strain almost vanished after decompression (Wu et al., 2005).

In this paper, a modified density-dependent DPC plasticity model was described. A nonlinear elasticity law as a function of the relative density and the stress was used to describe the unloading behaviour during pharmaceutical powder compaction. To identify the material parameters of the modified DPC model, a new experimental calibration procedure was also developed, based on the uniaxial compaction test using an instrumented die. This modified DPC model with the nonlinear elasticity law was implemented in ABAQUS by using user subroutines.

The rest of this paper is organised as follows: Section 2 describes typical experimental tests used to characterise the compaction behaviour of pharmaceutical powders using an instrumented die, and to measure the strengths of the resulting tablets; Section 3 presents a modified density-dependent Drucker-Prager Cap plasticity model with a nonlinear elasticity law to represent the compaction behaviour; Section 4 introduces the calibration method based on the experimental tests described in Section 2; Section 5 presents results for the calibrated material parameters of MCC Avicel PH101 powders, the experimental validation of the model and some qualitative analyses of tablet failure using numerical simulations. Finally, Section 6 summarises the conclusions.

2. Characterising compaction behaviour of pharmaceutical powders

To characterise the compaction behaviour of powders, both triaxial equipment and uniaxial die compaction equipment have been used (Pavier and Doremus, 1999; Rottmann et al., 2001). Triaxal equipment allows testing with different loading paths by introducing both the shear and compressive stresses in the compact and can characterise more complete mechanical properties of powders, but it is more complex, expensive and difficult to use. By comparison, uniaxial die compaction equipment is much cheaper and easier to use. Moreover, it better models the industrial process of tabletting. Therefore, uniaxial die compaction equipment, also known as compaction simulators in the pharmaceutical industry, have been widely used to investigate the compaction behaviour of pharmaceutical powders (Doelker and Massuelle, 2004). To measure the radial die wall pressure and investigate the powder friction at the die wall during compaction, instrumented dies are generally equipped to compaction simulators for tabletting research and development (Doelker and Massuelle, 2004). The axial upper/lower punch forces and displacements, and the radial die wall pressure are measured during compaction (see Fig. 1).

Fig. 2 shows the typical quasi-static compaction behaviour of MCC Avicel PH101 measured by a compaction simulator equipped with an 8 mm instrumented die (Phoenix Calibration & Services Ltd, Bobbington, UK) at a compaction speed of 0.1 mm/s. The axial stress, σ_z^U, was calculated from the upper punch force divided by the cross-section area of the compact; the axial strain, ε_z, was calculated from the powder height change (ΔH) divided by its initial filling height (H_0) in the die. Both the loading and unloading curves exhibit nonlinear behaviour. Moreover, the unloading curves at different compaction densities (or heights) are not parallel, i.e. the unloading properties are density-dependent. The axial to radial stress transmission during unloading (Fig. 2b), related to Poisson's ratio, also shows nonlinear behaviour. Note that the density value shown in Fig. 2 is the compaction density calculated from the powder weight divided by the in-die powder volume.

During compaction, the powder friction at the die wall induces non-uniform axial stress and produces density gradients within the compact. The friction effect could be quantified by the wall friction coefficient during compaction. Based on Janssen-Walker theory (Nedderman, 1992), the wall friction coefficient was calculated as:

$$\mu = \frac{D}{4H}\frac{\sigma_Z^L}{\sigma_r(Z)}\left(\frac{\sigma_z^U}{\sigma_z^L}\right)^{\frac{z}{H}}\ln\left(\frac{\sigma_z^U}{\sigma_z^L}\right) \tag{1}$$

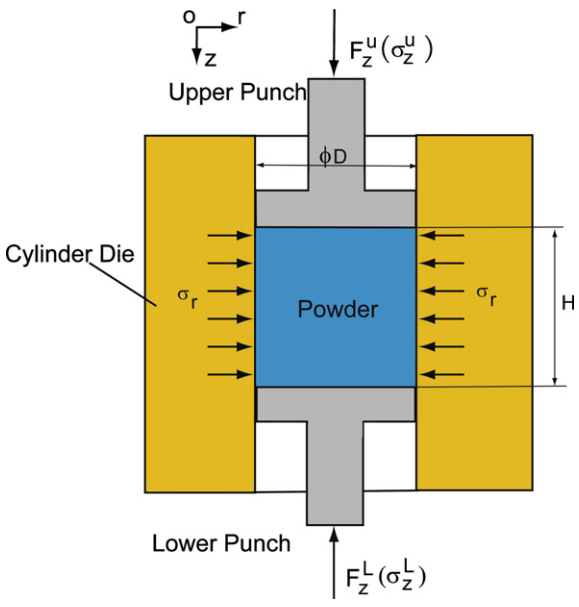

Fig. 1. 2D diagram of an instrumented die.

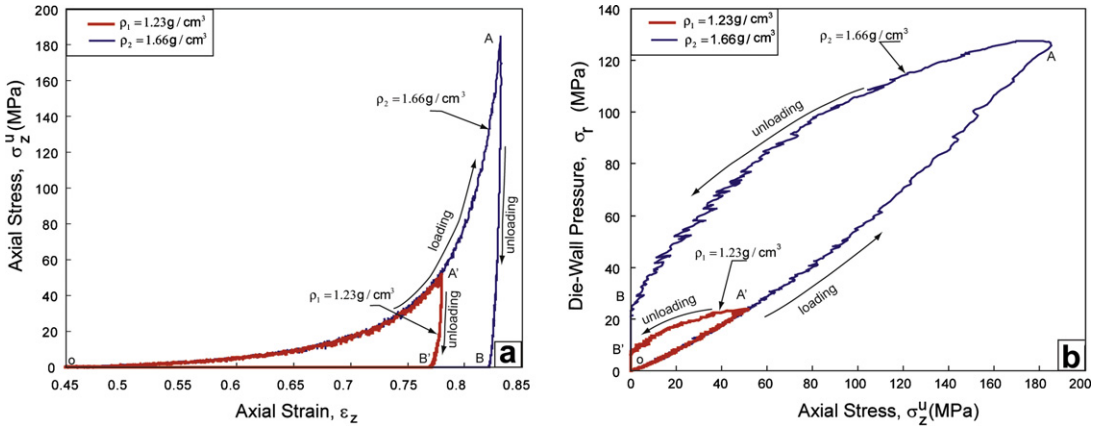

Fig. 2. Typical quasi-static compaction behaviour of MCC Avicel PH101 at different compaction densities: (a) typical axial stress–strain relation; (b) typical stress transmission from axial stress to radial wall pressure.

where D is the die interior diameter, H is the compaction height in the die, $\sigma_r(z)$ is the radial pressure at the position z from the top surface of the powder compact, and σ_z^U and σ_z^L are axial compression stresses applied by the upper and lower punches, respectively.

In order to obtain the intrinsic characteristics of the powder, the influence of die wall friction should be minimised. Two kinds of lubrication methods could be used: the external lubrication method and the internal lubrication method. In the internal lubrication method, magnesium stearate (e.g. 1% w/w) was mixed with powders, while in the external lubrication method the suspension of magnesium stearate was used to lubricate the die wall. Fig. 3 shows the die wall friction coefficient change with the applied upper-punch force at the position where the wall pressure sensor was located. It was found that both lubrication methods could reduce the die wall friction coefficient to a small value (e.g. 0.12) during the compaction of MCC Avicel PH101. It was generally considered that a die wall friction coefficient of order 0.1 should have a small effect on powder compaction behaviour (Cunningham et al., 2004).

After the tablets made by compaction simulators are ejected from the die, their strengths can be measured. Typically, the radial tensile strength and the axial compressive/tensile strengths of pharmaceutical tablets are measured because of relatively simple experimental procedures. The radial tensile strength of tablets is measured using a diametrical compression test (also known as Brazilian disk test), as shown in Fig. 4a. Tablets are crushed along their central lines. From the maximum crush force, the radial tensile strength of tablets is determined using the following equation:

$$\sigma_d^f = \frac{2F_{\max}}{\pi D t} \tag{2}$$

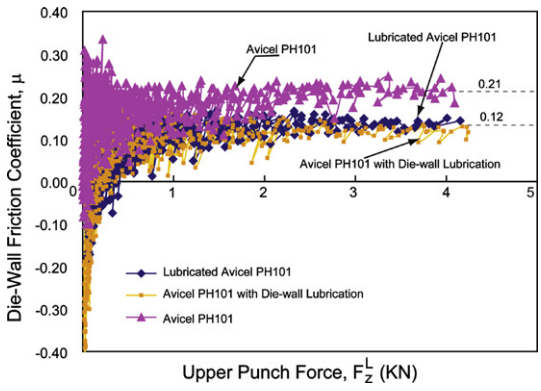

Fig. 3. Lubrication effect on die wall friction.

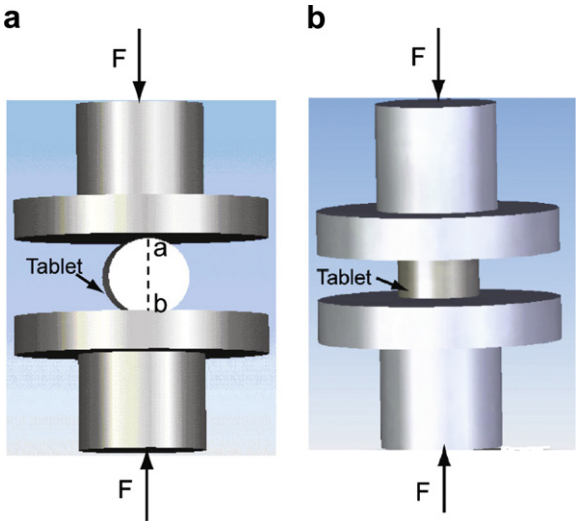

Fig. 4. Tablet strength measurement: (a) radial tensile strength; (b) axial compressive/tensile strength.

where $F_{\max}$ is the crushing force, D is the tablet diameter and t is the tablet thickness. In order to use Eq. (2), the failure model of tablets should be brittle fracture, that is, tablets should be split into two halves along the centre line (see dashed line 'ab' in Fig. 4a). The axial compressive/tensile strengths are measured by uniaxial compression/tension tests, as shown in Fig. 4b. The tablet is compressed/stretched axially. The axial compression strength is calculated from:

$$\sigma_c^f = \frac{4F_y}{\pi D^2} \tag{3}$$

where F_y is the axial compression force at the yield point.

3. Modified Drucker-Prager Cap model

Since being first introduced by Drucker et al. (1957), the DPC plasticity model has been modified and expanded over the years (Chen and Mizuno, 1990; Sandler, 2002). Fig. 5 shows a typical Drucker-Prager Cap model (ABAQUS, 2006). The model is assumed to be isotropic and its yield surface includes three segments: a shear failure surface, providing dominantly shearing flow, a "cap," providing an inelastic hard-

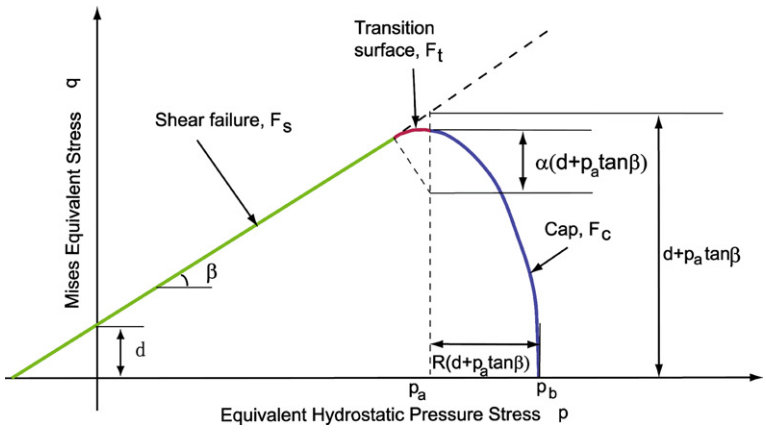

Fig. 5. Drucker-Prager Cap model: yield surface in the $p - q$ plane.

ening mechanism to represent plastic compaction, and a transition region between these segments, introduced to provide a smooth surface purely for facilitating the numerical implementation. Since the material parameters of pharmaceutical powders are density-dependent (Cunningham et al., 2004; Jonsén and Häggblad, 2005), a modified density-dependent Drucker-Prager Cap model is adopted to describe the mechanical behaviour of pharmaceutical powders in this work. Further, a nonlinear elasticity law was proposed to describe the unloading behaviour. Elastic parameters, the bulk modulus, K, and shear modulus, G, were expressed as functions of the relative density and stress level, rather than constants. Fig. 6 shows a schematic representation of a density-dependent DPC model, where ρ is the relative density of the compact. Because of the axisymmetry, only one quarter of the full 3D yield surface is plotted in the principal stress space, as shown in Fig. 6a; the symmetry axis is $\sigma_1 = \sigma_2 = \sigma_3$ in which σ_1, σ_2 and σ_3 are the principal stresses.

3.1. Formulas and material parameters

The Drucker-Prager shear failure surface is written as:

$$F_s = q - p\ \tan\beta - d = 0 \tag{4}$$

where β is the material friction angle, d is its cohesion, $p = -\frac{1}{3}\mathrm{trace}(\boldsymbol{\sigma})$ is the hydrostatic pressure stress, and $q = \sqrt{\frac{3}{2}(\mathbf{S}:\mathbf{S})}$ is the Mises equivalent stress in which $\mathbf{S}$ is the stress deviator, defined as:

$$\mathbf{S} = \boldsymbol{\sigma} + p\mathbf{I} \tag{5}$$

where $\boldsymbol{\sigma}$ is the stress tensor, and $\mathbf{I}$ is the identity matrix.

For a uniaxial cylindrical die compaction test, the hydrostatic pressure stress and the Mises equivalent stress are expressed as:

$$p = -\frac{1}{3}(\sigma_z + 2\sigma_r) \tag{6}$$

$$q = |\sigma_z - \sigma_r| \tag{7}$$

where σ_z and σ_r are the axial and radial stresses, respectively.

The cap serves two main purposes: it bounds the yield surface in hydrostatic compression, thus providing an inelastic hardening mechanism to represent plastic compaction, and it helps to control volume dilatancy when the material yields in shear by providing softening as a function of the inelastic volume increase created as the material yields on the Drucker-Prager shear failure and transition yield surfaces. The cap surface hard-

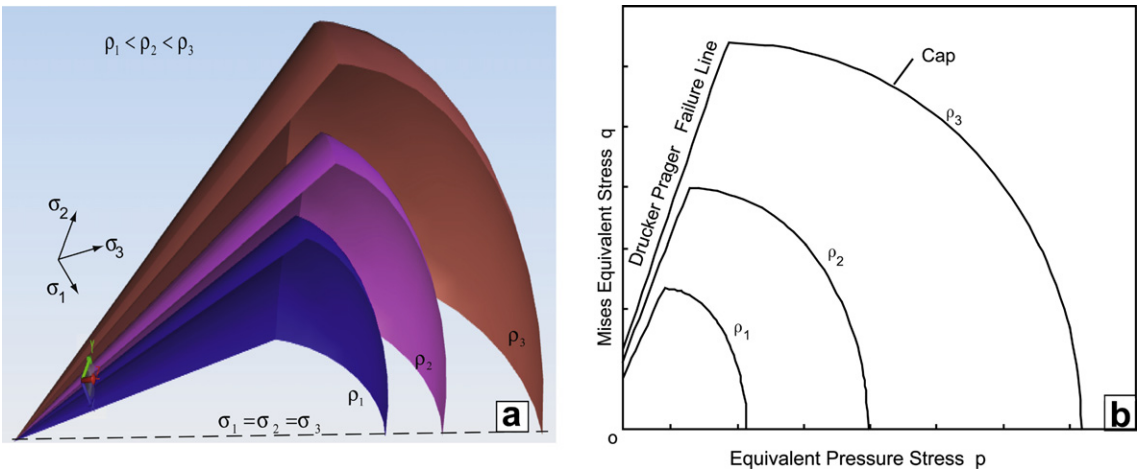

Fig. 6. Schematics of a density-dependent Drucker-Prager Cap model: (a) 3D yield surfaces in principal stress space (1/4 model); (b) 2D representation.

ens or softens as a function of the volumetric plastic strain: volumetric plastic compaction (when yielding on the cap) causes hardening, while volumetric plastic dilation (when yielding on the shear failure surface) causes softening. The cap yield surface is written as:

$$F_c = \sqrt{(p - p_a)^2 + \left[\frac{Rq}{1 + \alpha - \alpha/\cos\beta}\right]^2} - R(d + p_a \tan\beta) = 0 \tag{8}$$

where R is a material parameter (between 0.0001 and 1000.0) that controls the shape of the cap, α is a small number (typically 0.01–0.05) used to define a smooth transition surface between the shear failure surface and the cap, and p_a is an evolution parameter that represents the volumetric plastic strain driven hardening/softening. The hardening/softening law is a user-defined piecewise linear function relating the hydrostatic compression yield stress, p_b, and the corresponding volumetric inelastic (plastic and/or creep) strain. Here, only volumetric plastic strain ε_v^p is considered, we have:

$$p_b = f(\varepsilon_v^p) \tag{9}$$

The volumetric plastic strain can be expressed as (Chtourou et al., 2002):

$$\varepsilon_v^p = \ln\left(\frac{\rho}{\rho_0}\right) \tag{10}$$

where ρ is the current relative density, and ρ_0 is the initial relative density on filling of die. The evolution parameter p_a is given as:

$$p_a = \frac{p_b - Rd}{(1 + R\tan\beta)} \tag{11}$$

The transition surface is defined as:

$$F_t = \sqrt{[(p - p_a)]^2 + \left[q - \left(1 - \frac{\alpha}{\cos\beta}\right)(d + p_a \tan\beta)\right]^2} - \alpha(d + p_a \tan\beta) = 0 \tag{12}$$

To determine the plastic flow rule, the plastic potential is defined by an associated component (that is, a potential function G_c that is equivalent to the cap yield surface F_c) on the cap and a non-associated component on the failure and transition regions. The associated flow potential component in the cap region is defined as:

$$G_c = \sqrt{(p - p_a)^2 + \left[\frac{Rq}{1 + \alpha - \alpha/\cos\beta}\right]^2} \tag{13}$$

The non-associated flow component in the failure and transition regions is defined as:

$$G_s = \sqrt{[(p_a - p)\tan\beta]^2 + \left[\frac{q}{1 + \alpha - \alpha/\cos\beta}\right]^2} \tag{14}$$

The two elliptical portions, G_c and G_s, form a continuous and smooth potential surface.

Considering the associated flow rule, we can write the inelastic strain rate in the cap region as:

$$\dot{\varepsilon}_{ij}^p = \dot{\lambda}\frac{\partial G_c}{\partial \sigma_{ij}} = \dot{\lambda}\frac{\partial F_c}{\partial \sigma_{ij}} \tag{15}$$

where $\dot{\lambda}$ is a positive scalar denoting the magnitude of the plastic deformation, and $\frac{\partial G_c}{\partial \sigma}$ denotes the direction of the plastic flow.

To uniquely define each of the yield surfaces, six parameters are required: β, d, p_a, R, p_b and α, for which β, d, R and p_a are functions of the relative density. The friction angle β and cohesion d are needed to define the Drucker-Prager shear failure surface; the cap eccentricity parameter R and evolution p_a are required to define the cap surface, and p_b as a function of the volumetric plastic strain is required to define the cap hardening/softening law; α is required to define the transition surface.

3.2. Nonlinear elasticity law

Experimental measurements on real pharmaceutical powders exhibit nonlinear behaviour during unloading. As shown in Fig. 2, there exist nonlinear segments at the end of the unloading curves, which become more obvious for a relatively loose compact. Some researchers (Aydin et al., 1996; Wu et al., 2005) considered that the nonlinear segments of the unloading curves were a result of dilation during unloading; that is, the unloading path intersected with the Drucker-Prager failure surface F_s before the axial stress decreased to zero. Using this assumption to define the Drucker-Prager failure surface resulted in an unrealistic simulation of decompression during die compaction, in which the plastic strain almost vanished after decompression due to the dilation of powders (Wu et al., 2005), that is, the tablet was not formed, which was obviously not true in the experimental tests on pharmaceutical powders. To avoid this problem, we use a nonlinear elasticity law rather than a linear elasticity law to describe the unloading behaviour, a similar method for describing geomaterials (Chen and Mizuno, 1990) and metal powders (Coube and Riedel, 2000). During unloading and reloading in the die compaction, lactose, an excipient widely used for the failure mechanism investigation of tablets exhibited a very small hysteresis, and MCC Avicel PH101 also showed a relatively small hysteresis at higher compaction densities (typically 0.85 for pharmaceutical tablets). Therefore, the nonlinear elasticity assumption is suitable. Within the elastic range, the elastic behaviour of the material must be path-independent in order not to generate hysteresis. To satisfy the path independency, the bulk modulus, K, and shear modulus, G, could be expressed as (Chen and Baladi, 1985):

$$K = K(I_1, \rho) = K(p, \rho) \tag{16}$$

$$G = G\left(\sqrt{J_2}, \rho\right) = G(q, \rho) \tag{17}$$

where $I_1 = 3p$ is the first stress invariant, $\sqrt{J_2} = q/\sqrt{3}$ is the second stress invariant and ρ is the density. In the DPC model, materials behave isotropically and elastically during unloading, therefore, the elastic material moduli, K and G, can be obtained by using the unloading data of the hydrostatic loading test, the triaxial test, the uniaxial strain test, and so on. In the elastic range, the behaviour of isotropic materials is governed by the incremental Hooke' law:

$$d\varepsilon_{\mathbf{ij}}^{\mathbf{e}} = \frac{dI_1}{9K}\delta_{\mathbf{ij}} + \frac{ds_{\mathbf{ij}}}{2G} \tag{18}$$

where $d\varepsilon_{\mathbf{ij}}^{\mathbf{e}}$ is the elastic strain increment, $s_{\mathbf{ij}} = \sigma_{\mathbf{ij}} - (I_1/3)\delta_{\mathbf{ij}}$ is the deviatoric stress tensor, and $\delta_{\mathbf{ij}}$ is the Kronecker delta.

For the uniaxial strain test (or uniaxial compaction test), the following relations are obtained:

$$\dot{\varepsilon}_r = \dot{\varepsilon}_\theta = 0 \tag{19}$$

and

$$\sigma_r = \sigma_\theta \tag{20}$$

Thus, from Eq. (18), the axial strain increment during unloading can be expressed as:

$$d\varepsilon_z = \frac{d\sigma_z + 2d\sigma_r}{3K} = \frac{dI_1}{3K} = \frac{dp}{K} \tag{21}$$

$$d\varepsilon_z = \frac{d\sigma_z - d\sigma_r}{2G} = \frac{dq}{2G} \tag{22}$$

Consequently, the bulk modulus K can be obtained from the hydrostatic pressure/axial strain unloading curve and may be fitted as a function of p. The shear modulus G can be obtained from the equivalent-Mises-stress/axial strain unloading curve and may be fitted as a function of q.

4. Material parameter identification for the DPC model

Typically, triaxial equipment has been used to calibrate the DPC model (Rottmann et al., 2001). However, triaxial equipment is complex and difficult to use in practical engineering applications. Therefore, a calibration

method based on experimental tests from compaction simulators with an instrumented die is developed to identify the material parameters of the modified DPC model. As described in Section 3.1, six parameters are required to define the yield surface of the modified DPC model: β, d, p_a, R, p_b and α. In addition, two elastic parameters, Young's modulus E and Poisson's ratio v, are required for describing the elastic behaviour of powders. We now describe how to obtain these parameters from uniaxial compaction experiments using a compaction simulator.

4.1. Parameters for yield surfaces

The Drucker-Prager shear failure surface could be determined by assuming that the nonlinear segment of the unloading curve in a die compaction test was produced by the shear failure (Aydin et al., 1996; Sandler et al., 1976; Wu et al., 2005). The nonlinear unloading segment of the unloading curve, line CD as shown in Fig. 7b, will locate on the shear failure line in the $p-q$ space, as shown in Fig. 7a. Consequently, the shear failure surface can be determined by plotting a straight line through CD. This method is very simple, but it may result in an unrealistic simulation of decompression when material parameters calibrated by this method are used (Wu et al., 2005), due to the dilation of the material during unloading when the unloading path hits the shear failure line.

Here, we employed another method (Procopio et al., 2003) to determine the Drucker-Prager shear failure surface by using any two of four experiments for measuring the tablet strengths: the uniaxial tension, pure shear, diametrical compression and uniaxial compression tests. First, the loading paths of the four kinds of tests above were plotted in the $p-q$ space. Under the elastic loading, these four loading paths can be presented by four dashed lines through the origin, point O, whose slopes are -3, ∞, $3\sqrt{13}/2$ and 3, respectively, as shown in Fig. 8. Then, the four maximum loading points corresponding to four kinds of the tablet strengths are plotted on these four dashed lines, respectively. Finally, the shear failure line can be determined by plotting a straight line though any two maximum loading points. The slope of the line gives the friction angle β, and the intersection with q axis gives the cohesion d. Here, we used two simple tests: the diametrical compression test and the uniaxial compression test. The equivalent hydrostatic pressure stress p and Mises equivalent stress q are $p=\frac{2}{3}\sigma_d^f, q=\sqrt{13}\sigma_d^f$ for the diametrical compression test, and $p=-\frac{1}{3}\sigma_c^f, q=-\sigma_c^f$ for the uniaxial compression test, respectively. Consequently, the cohesion d and friction angle β are expressed as:

$$d=\frac{\sigma_c^f\sigma_d^f(\sqrt{13}-2)}{\sigma_c^f+2\sigma_d^f} \tag{23}$$

$$\beta=\tan^{-1}\left[\frac{3(\sigma_c^f+d)}{\sigma_c^f}\right] \tag{24}$$

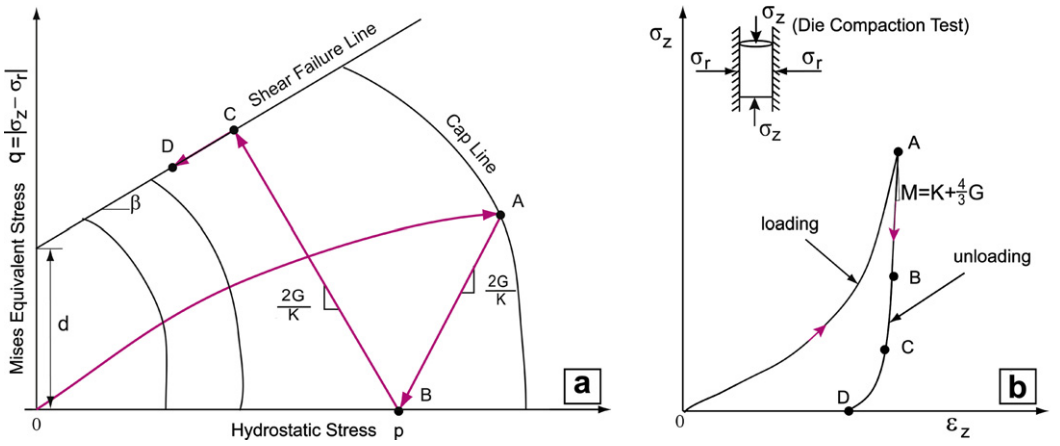

Fig. 7. A method to determine shear failure line from die compaction tests (Aydin et al., 1997): (a) loading path plotted on the $p-q$ space; (b) axial stress–axial strain curve.

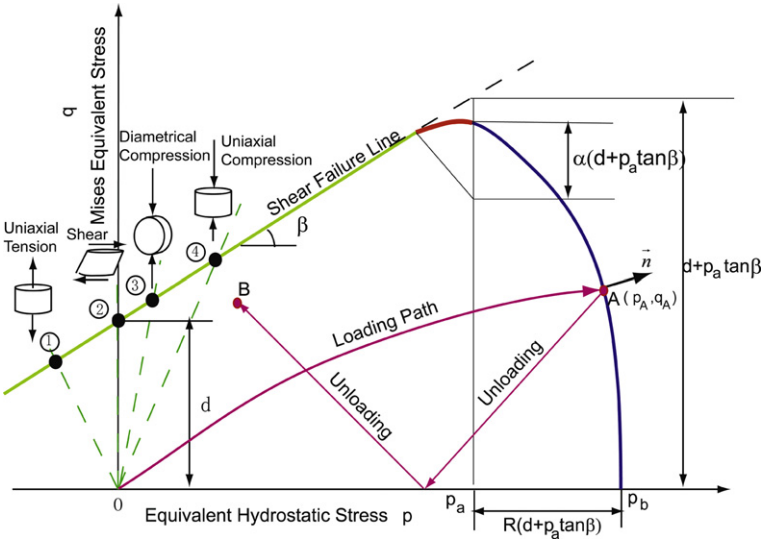

Fig. 8. Determination of shear failure line from tablet strength tests.

where σ_d^f is the radial tensile strength of tablets measured from the diametrical test, and σ_c^f is the axial compressive strength of tablets measured from the uniaxial compression test.

To define the cap yield surface (Eq. (8)), four parameters, p_a, R, p_b and α, are required. α is a small number between 0.01 and 0.05; here we set it to 0.02. p_a and R can be determined by analysing the stress state of the loading points on the cap surface. As shown in Fig. 8, the loading path OA is plotted at the $p-q$ space. At the loading point located at the cap surface, e.g. point A, cap yielding is active, that is, Eq. (8) is satisfied:

$$F_c(p_A, q_A) = 0 \tag{25}$$

With an assumption that the die wall is a rigid body without any deformation in the cylindrical die compaction test, the radial plastic strain rate at Point A (Eq. (15)) can be written as:

$$\dot{\varepsilon}_r^p = \dot{\lambda}\frac{\partial G_c}{\partial \sigma_r}\bigg|_{(p_A,q_A)} = 0 \tag{26}$$

Since $\dot{\lambda}$ is a positive quantity, then

$$\frac{\partial G_c}{\partial \sigma_r}\bigg|_{(p_A,q_A)} = 0 \tag{27}$$

By using Eqs. (13) and (27) can be rewritten as:

$$2(p-p_a)\frac{\partial p}{\partial \sigma_r}\bigg|_{(p_A,q_A)} + 2\frac{R^2 q}{(1+\alpha-\alpha/\cos\beta)^2}\frac{\partial q}{\partial \sigma_r}\bigg|_{(p_A,q_A)} = 0 \tag{28}$$

Considering $p = -\frac{1}{3}(\sigma_z + 2\sigma_r)$ and $q = |\sigma_z - \sigma_r|$, we can rewrite Eq. (28) as:

$$-\frac{2}{3}(p_A - p_a) + \frac{R^2 q_A}{(1+\alpha-\alpha/\cos\beta)^2} = 0 \tag{29}$$

From Eq. (29), the cap shape parameter R is given as:

$$R = \sqrt{\frac{2(1+\alpha-\alpha/\cos\beta)^2}{3q_A}(p_A - p_a)} \tag{30}$$

Consequently, the evolution parameter p_a can be obtained from Eqs. (8) and (30) as:

$$p_a = -\frac{[3q_A + 4d\tan\beta(1+\alpha-\alpha/\cos\beta)^2]}{4[(1+\alpha-\alpha/\cos\beta)\tan\beta]^2} + \frac{\sqrt{9q_A^2 + 24dq_A(1+\alpha-\alpha/\cos\beta)^2\tan\beta + 8(3p_Aq_A + 2q_A^2)[(1+\alpha-\alpha/\cos\beta)\tan\beta]^2}}{4[(1+\alpha-\alpha/\cos\beta)\tan\beta]^2} \tag{31}$$

Once the powder was compacted to a specified height (e.g. Point A shown in Fig. 8), the applied force was released and the tablet was then ejected from the die. The relative density of the tablet can be calculated from the measured tablet density after ejection divided by the initial filling density of powders. With the measured relative density, the volumetric plastic strain ε_v^p at the loading point in the $p-q$ space can be calculated from Eq. (10), and p_b can be calculated from Eq. (11). The cap hardening/softening law can be obtained by plotting p_b as a function of a volumetric plastic strain ε_v^p.

4.2. Elastic parameters

In the DPC model, the Young's modulus E and Poisson's ratio v are required, which have the relations with the bulk modulus and shear modulus as:

$$G = \frac{E}{2(1+v)} \tag{32}$$

$$K = \frac{E}{3(1-2v)} \tag{33}$$

For a die compaction test, the strain increment and elastic strain increment relation during unloading may be obtained by combining Eqs. (21) and (22) and expressed as:

$$d\sigma_z = Md\varepsilon_z = \left(K + \frac{4}{3}G\right)d\varepsilon_z \tag{34}$$

and the axial stress increment and radial stress increment relation may be written as:

$$d\sigma_z = \frac{3K+4G}{3K-2G}d\sigma_r \tag{35}$$

in which M is the constrained modulus. Substitution of Eqs. (32) and (33) into Eqs. (34) and (35) yields:

$$d\sigma_z = \frac{E(1-v)}{(1+v)(1-2v)}d\varepsilon_z \tag{36}$$

$$d\sigma_z = \frac{1-v}{v}d\sigma_r \tag{37}$$

Thus, using Eq. (37), we can obtain the Poisson's ratio v as a function of the axial stress, σ_z, and the relative density of compact, ρ, from the axial stress/radial stress unloading curve (see Fig. 2b). Consequently, using Eq. (36) and the Poisson's ratio obtained, we can obtain the Young's modulus E as a function of the axial stress, σ_z, and the relative density of compact, ρ, from the axial stress/axial strain unloading curve (see Fig. 2a).

5. Results

5.1. Material parameters of MCC Avicel PH101

The material parameter identification for MCC Avicel PH101 was performed by the method proposed in Section 4. The powder was uniaxially compacted by a high speed compaction simulator (Phoenix Calibration & Services Ltd, Bobbington, UK). An 8 mm diameter instrumented die was used to measure the radial wall pressure. As mentioned previously, to obtain the intrinsic material properties of pharmaceutical powders from die compaction tests, the wall friction influence should be minimised. Hence, MCC Avicel PH101 (FMC, UK)

was chosen in this study, due to its good self-lubrication performance. To further reduce the die wall friction effect, Avicel PH101 was mixed with 1% w/w magnesium stearate (Mallinckrodt, UK), which is normally used as a lubricant in a direct compression formulation. Table 1 lists material properties of MCC Avicel PH101 and magnesium stearate. A series of tablets with different densities were made by compressing powders to different specified heights in the die at a compaction speed of 0.1 mm/s. After ejection, the weight and dimensions of tablets were measured to calculate their densities. The axial tensile and axial compressive strengths of tablets were measured by the diametrical test and uniaxial simple compression test, respectively.

Typical loading–unloading curves of quasi-static uniaxial single-ended compaction tests of lubricated MCC Avicel PH101 are shown in Fig. 9. A piecewise linear function can be used to represent the unloading curve. For the sake of simplicity and easy numerical implementation, we use two linear segments to approximately describe the nonlinear unloading curve, for example, we use lines AC and CB to represent the unloading curve AA′B, as shown in Fig. 9. Consequently, Young's modulus and Poisson's ratio are represented as step functions of the axial stress, σ_z; that is, the Young's modulus and Poisson's ratio have two different values at the high stress segment and low stress segment of unloading curves, and the stress threshold (e.g. point C in Fig. 9) to separate the high stress segment from the low stress segment is determined from the curve fitting. For example, for the test shown in Fig. 9, at the high stress segment, AC, ($\sigma_z > 105$ MPa), the Young's modulus and Poisson's ratio are 22.6 GPa, and 0.233, respectively; at the low stress segment, CB ($\sigma_z \leqslant 105$ MPa), the Young's modulus and Poisson's ratio are 4.2 GPa, and 0.42, respectively. Figs. 10 and 11 illustrate the dependence of Poisson's ratio and Young's modulus on the relative density, respectively. With increasing relative density, both values of the Young's modulus and Poisson's ratio increase.

Fig. 12 shows the tablet strengths of Avicel PH101 measured by diametrical tests and uniaxial compression tests on tablets with different densities. The denser tablet has a higher strength. With the measured tablet strengths in Fig. 12, the cohesion, d, and friction angle, β, are calculated for each relative density, and plotted as functions of the relative density in Fig. 13. With the stress values of equivalent pressure stress p and Mises equivalent stress q at the largest compression point (e.g. Point A in Fig. 8), the parameters to define the cap surface, R, p_a and p_b, are determined, as shown in Fig. 14.

With all these parameters obtained, the modified DPC model can be fully defined.

Table 1
Material properties

Materials	Avicel PH101	Magnesium stearate	Lubricated Avicel PH101
Particle size (μm)	10–200	1–50	—
True density (g/cm^3)	1.577	—	1.4590

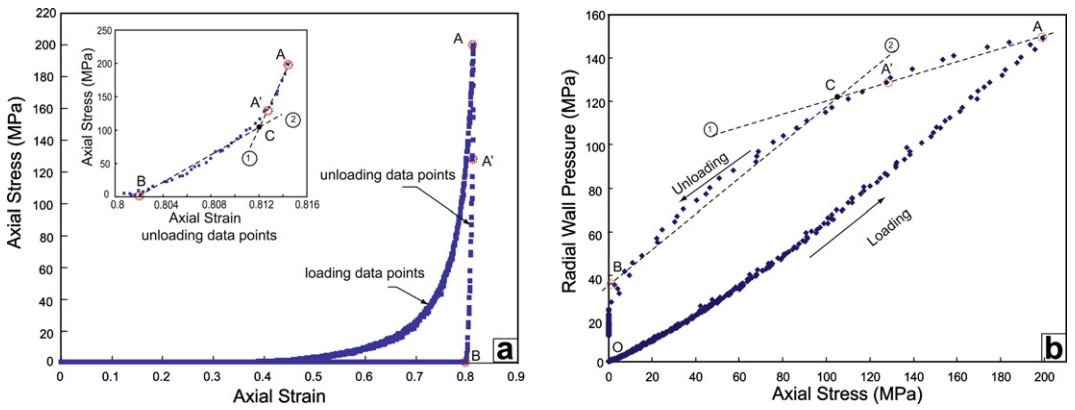

Fig. 9. Typical loading–unloading curves of lubricated Avicel PH101 in a die compaction test: (a) axial stress and axial strain relation; (b) axial stress transition to radial wall pressure.

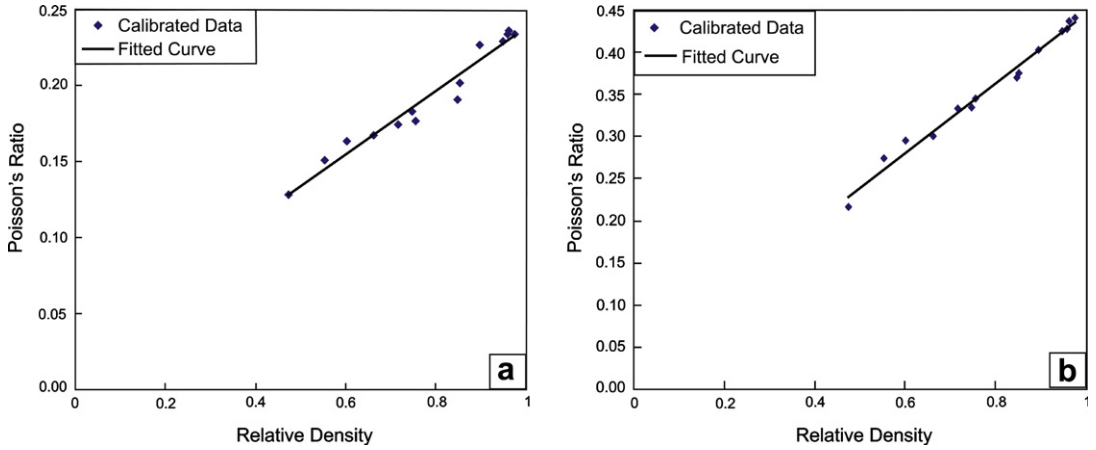

Fig. 10. Poisson's ratio as a function of relative density: (a) high stress segment of unloading curve; (b) low stress segment of unloading curve.

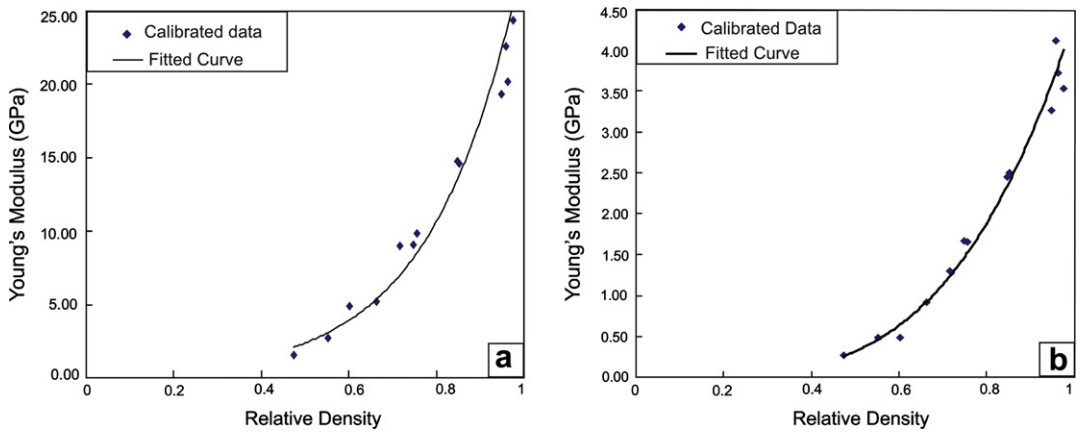

Fig. 11. Young's modulus plotted as a function of relative density: (a) high stress segment of unloading curve; (b) low stress segment of unloading curve.

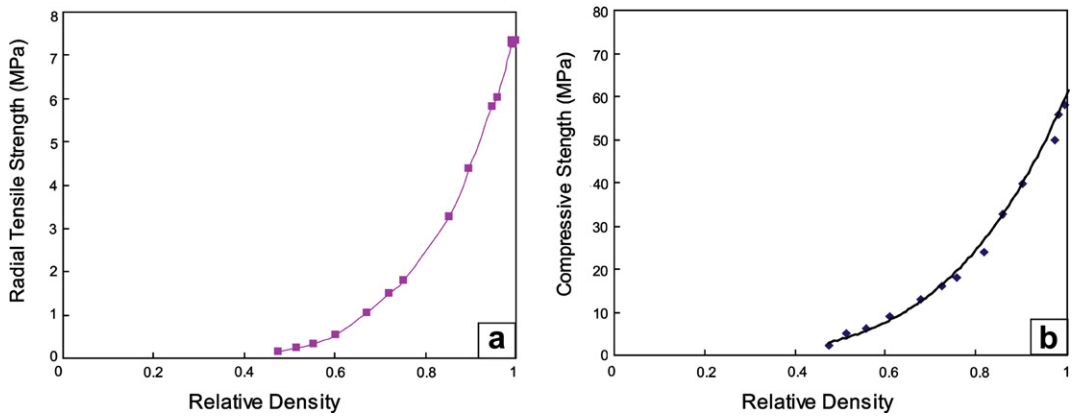

Fig. 12. Strengths of Avicel PH101 tablets: (a) radial tensile strength; (b) axial compressive strength.

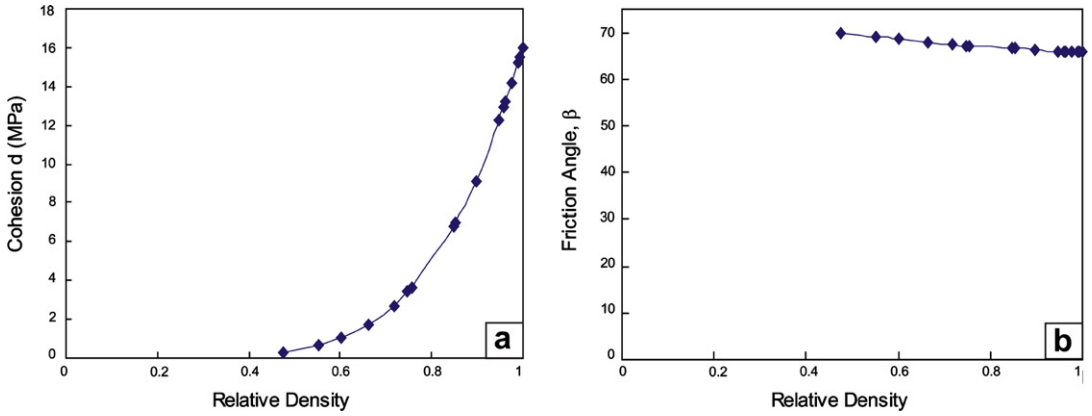

Fig. 13. (a) Cohesion and (b) friction angle plotted as functions of relative density.

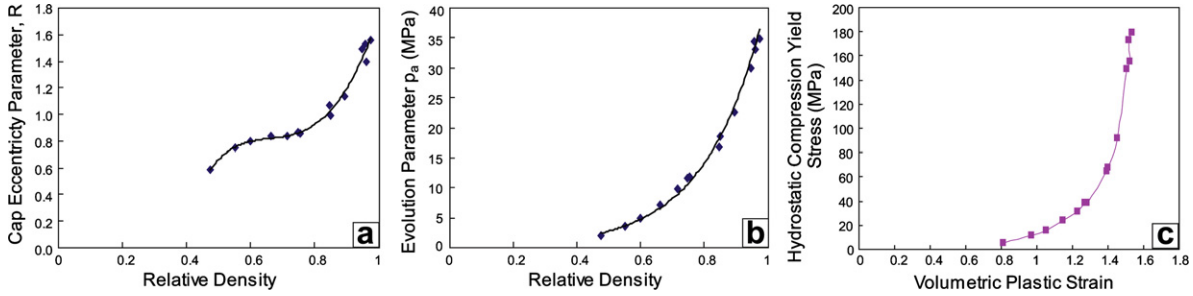

Fig. 14. Parameters for defining cap surface: (a) cap eccentricity parameter R; (b) evolution parameter; (c) hydrostatic compression yield stress.

5.2. Finite element modelling

Using materials parameters determined in Section 5.1, we employed ABAQUS/Standard to simulate the uniaxial single-ended die compaction process of MCC Avicel PH101 powders. Two kinds of tablets are considered, the flat-face tablet and concave tablets, where the concave tablet could be single radius concave (SRC) shaped or double radius concave (DRC) shaped. The modified Drucker-Prager Cap model was implemented in ABAQUS/Standard by using a user subroutine, USDFLD. Due to the axisymmetry of the geometry and the loading condition, an axisymmetrical model was adopted. The powder was modelled as a deformable continuum, while the upper/lower punches and die were modelled as analytical rigid bodies without any deformation. Fig. 15 shows finite element models and 2D meshes. Axisymmetric elements were used for modelling powders in the analyses. The wall friction effect was considered by adopting a Coulombic boundary condition on the interfaces of the powder die wall and the powder punch, and adjusted by changing the friction coefficient. In the simulations, first, powders in the die were compressed to a specified maximum compression height by an upper punch, then the upper punch was removed from the die to unload, and once the upper punch was moved out of the die, the lower punch was moved upward to eject the tablets.

First, uniaxial single-ended die compaction experiments for calibrating the model parameters were simulated, without considering wall friction. An 8 mm cylindrical die and flat-face punches were employed. Fig. 16a shows a comparison between experimental and calculated loading–unloading curves during the manufacture of 8 mm flat-face tablets. The loading–unloading curves from finite element analyses (FEAs) matched very well with experimental data. Note that the maximum compaction density was larger than the true density since the compaction density was calculated from the in-die compact height, which contained the elastic deformation. The maximum compaction force required for making a tablet with a specified density was also predicted. Again, Fig. 16b shows a good agreement between finite element predictions and experimental results.

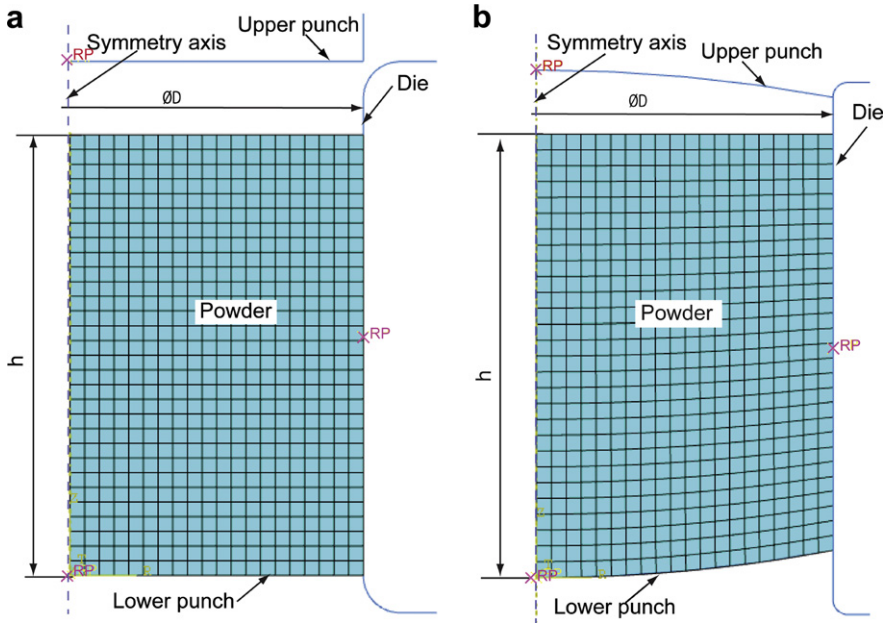

Fig. 15. Finite element model of die compaction using: (a) flat-face punches; (b) concave face punches.

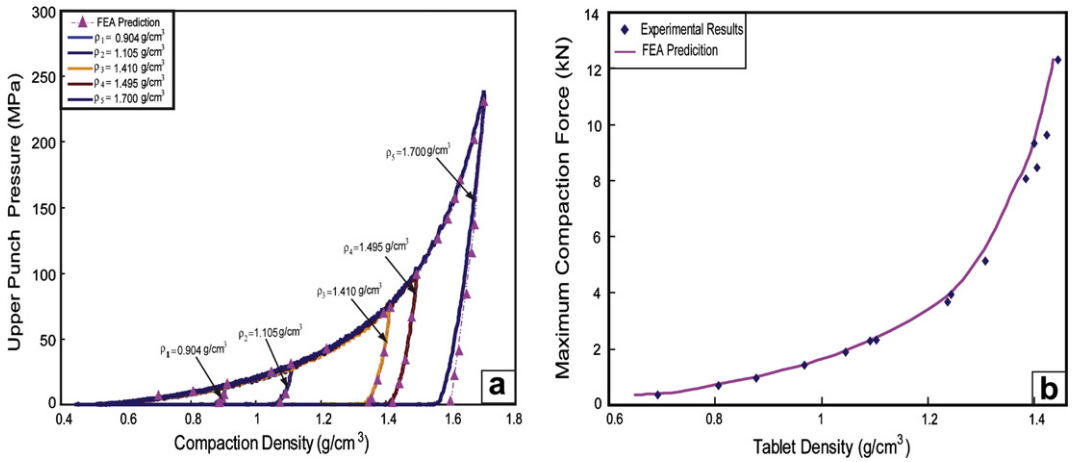

Fig. 16. A comparison between finite element simulation and experimental results of 8 mm flat-face tablets: (a) loading–unloading curves during compaction; (b) maximum compaction force.

To further assess the predictive capability of the model, besides 8 mm flat-face tablets used in the material parameter identification, tablets with other sizes and shapes were also investigated. Here, three different tablet shapes: flat-face (FF), single radius concave (SRC) and double radius concave (DRC), and two different tablet diameters: 8 and 11 mm, were considered. FEAs were used to predict the compaction behaviour of powders during the manufacture of these tablets. To facilitate comparison of different tablets, the mechanical response of powders during die compaction was described by the upper-punch pressure vs. average compaction density curve. The compaction pressure was calculated from the upper-punch force divided by the cross-sectional area of the die and the average compaction density was calculated from the mass of powder divided by its bulk volume. Fig. 17 shows a comparison of loading–unloading curves between finite element predictions and experimental results during tablet manufacture, where Fig. 17a is for 8 mm diameter FF, SRC and DRC tablets and Fig. 17b is for 11 mm diameter FF and SRC tablets. 8 mm tablets were made using two different pow-

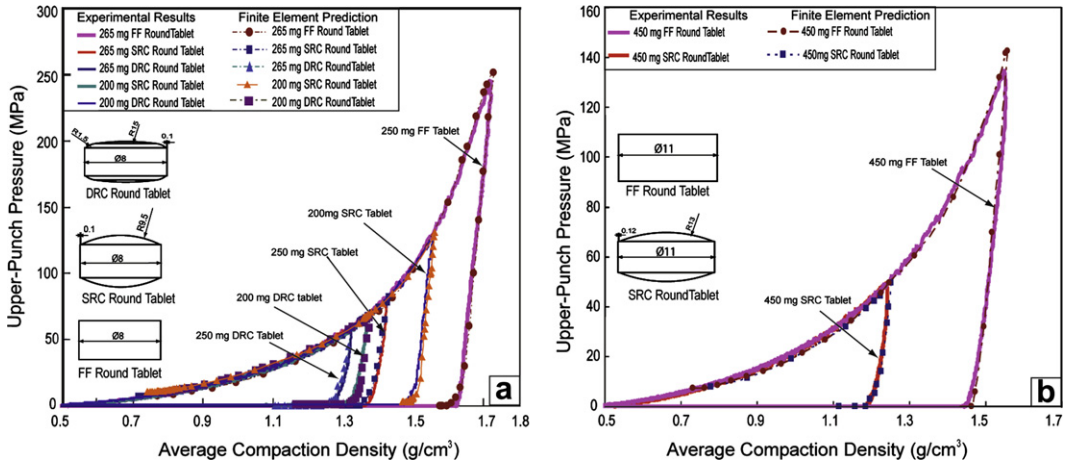

Fig. 17. Finite element prediction and experimental validation of unloading–loading curves: (a) 8 mm tablet; (b) 11 mm tablet.

der weights, 200 and 250 mg. Since the average compaction density was used as a parameter, the loading curves for these two different weight tablets should overlap, which was confirmed by both experimental and FEA results, as shown in Fig. 17. From Fig. 17, we can see that FEA results agreed well with the experimental results for both 8 and 11 mm flat-face and concave round tablets. The good agreement between FEA and experimental results showed that the model had a genuine predictive capability of powder compaction behaviour.

The numerical simulations could also be used to analyse the tablet failure mechanism. For demonstration, two typical tablet shapes, the flat-face and SRC, were chosen. In the following numerical simulations, powders with a 6 mm initial filling height were compressed to 2 mm. For a flat-face tablet without the wall friction effect, the stress distributions during tabletting are illustrated in Fig. 18. During the compression and decom-

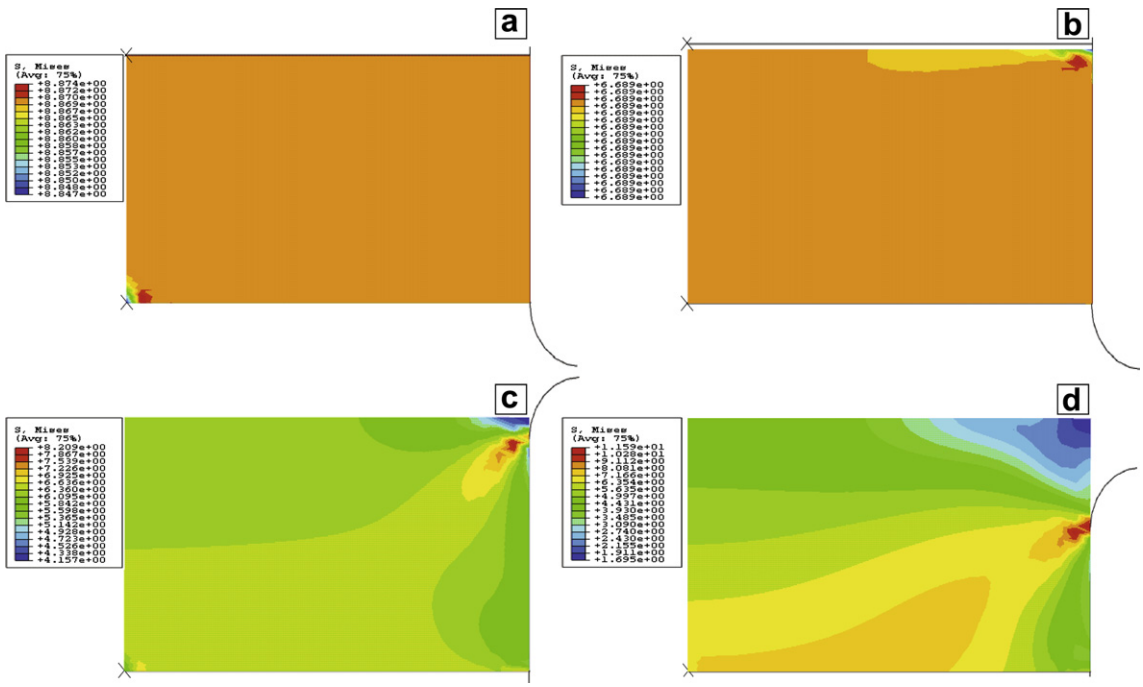

Fig. 18. Stress distribution of powders compacted by flat-face punches without wall friction: (a) maximum compaction; (b) after decompression; (c) emerging from the die; (d) during ejection.

pression phases, the stress distributions were uniform, and the density distributions were also uniform. During the ejection phase, a large stress concentration appeared near the die edge once the tablet emerged from the die, and large shear stresses developed due to the radial elastic recovery of the material of compacts outside the die. The local stress concentration may cause the capping and lamination failure. When wall friction was considered, the stress distributions during the compression and decompress phases were non-uniform, consequently, causing the density gradient. Fig. 19a shows a typical non-uniform density distribution of a flat-face compact when a wall friction coefficient of 0.2 is considered. The top corner had the highest density while the bottom corner had the lowest density, which was in agreement with experiments (Eiliazadeh et al., 2003). The punch geometry could also cause a non-uniform density distribution. Fig. 19b shows that a non-uniform density distribution of concave tablets, even without the wall friction effect. High density regions developed at the edges of the concave tablet with low density regions at the regions around the tablet apex, which was also consistent with experimental measurements (Eiliazadeh et al., 2003). Since the lowest density region in a flat-face tablet was at the bottom corner, as shown in Fig. 19a, it was therefore not surprising that concave tablets had more resistance against edge chipping, but less resistance against capping than flat-face tablets in practical manufacture processes of pharmaceutical tablets. Fig. 20 illustrates the stress distributions of compacts without the wall friction effect when concave surface punches are used. The stress distributions were always non-

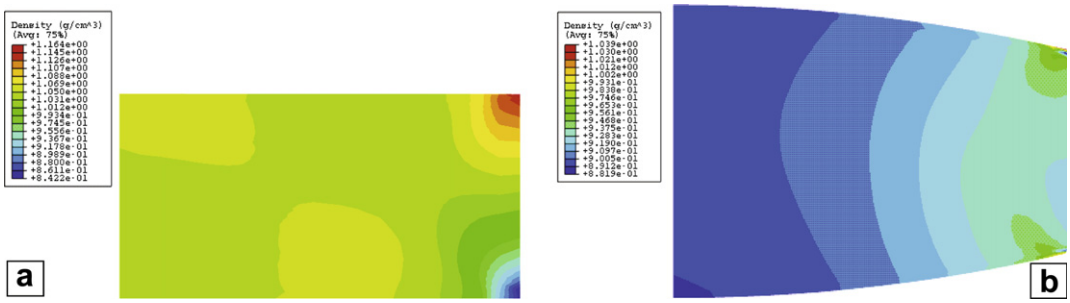

Fig. 19. Non-uniform density distribution of tablet due to (a) wall friction; (b) punch geometry.

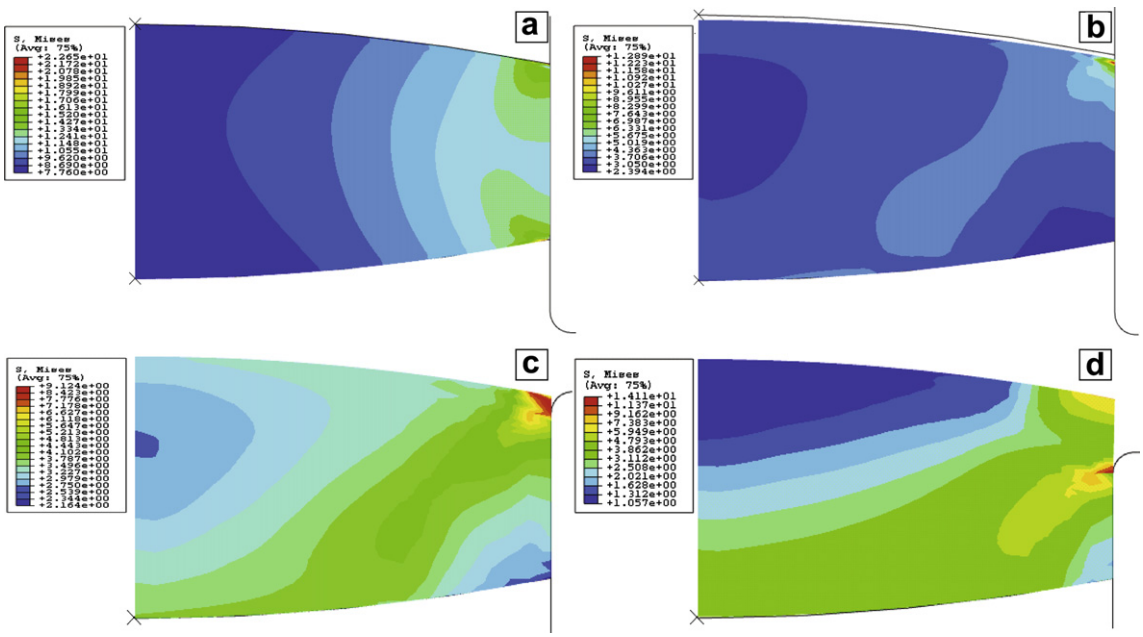

Fig. 20. Stress distribution during compaction using concave punches.

uniform during the compression, decompression and ejection phases. When the applied force from the upper punch was removed, the radial elastic recovery of the material at the top central region caused large shear stresses because most of other regions were still constrained by die walls, and developed larger stress concentrations at the top corner of the compact. This could also be used to explain the experimental observation that capping took place more frequently in concave tablets than in flat-face tablets. Similar to flat-face tablets, the stress concentration developed near the top corner during ejection due to the radial elastic recovery of the material of tablets outside the die. The stress concentration could contribute to capping and lamination.

6. Conclusions

The die compaction tests on pharmaceutical powders showed the nonlinearity of the unloading curve and the density dependence of compaction behaviour. By adopting a similar treatment as for geological materials, a nonlinear elasticity law was expressed as a function of the relative density and stress, used for describing the unloading behaviour of pharmaceutical powders. A density-dependent Drucker-Prager Cap model with the nonlinear elasticity model was proposed and implemented into ABAQUS/Standard by using a user subroutine (USDFLD). To determine the material parameters of the model from experiments, a material parameter identification method was proposed, based on the instrumented cylindrical die compaction test with flat-face punches and the tablet strength test. The model was validated by observing a good agreement between finite element prediction and experimental measurement of loading–unloading curves during the manufacture of flat-face, single radius concave and double radius concave round tablets. The detailed stress and density distributions of flat-face and the SRC round tablets during tabletting, including the compression, decompression and ejection phases, were analysed. FEA results showed that the density and stress distributions could be used to analyse and explain tablet defects such as edge chipping, capping and lamination. For example, non-uniform density distributions due to wall friction or the punch geometry could be used to explain the phenomena in the practical manufacture of pharmaceutical tablets that concave tablets had more resistance against edge chipping and less resistance against capping, compared with flat-face tablets. The local stress concentration and large shear stress due to the radial elastic recovery during the decompression and ejection phases could be used to analyse capping and laminar cracks. The results obtained so far indicate the model has a great potential for the tabletting process modelling of pharmaceutical powders and the failure investigation of tablets. Furthermore, the equipment and procedures for carrying out parameterization are readily available to the pharmaceutical industry.

Acknowledgments

This work was undertaken in the Pfizer Institute for Pharmaceutical Materials Science in Cambridge, and the research funding by Pfizer Global R&D is gratefully acknowledged. The authors also thank Dr. Gary Nichols for his assistance with SEM imaging, and Dr. Hussein for help conducting the experiments.

References

ABAQUS, 2006. ABAQUS 6.6 Theory Manual. ABAQUS Inc.

Aydin, I., Briscoe, B.J., Ozkan, N., 1997. Modelling of powder compaction: a review. MRS Bulletin, 45–51.

Aydin, I., Briscoe, B.J., Sanliturk, K.Y., 1996. The internal form of compacted ceramic components: a comparison of a finite element modelling with experiment. Powder Technology 89, 239–254.

Burlinson, H., 1968. Tablets and Tabletting. William Heinemann Medical Books Ltd, London.

Chen, W.F., Baladi, G.Y., 1985. Soil Plasticity: Theory and Implementation. Elsevier, New York.

Chen, W.F., Mizuno, E., 1990. Nonlinear Analysis in Soil Mechanics: Theory and Implementation. Elsevier Science Publishing Company Inc., New York.

Chtourou, H., Guillot, M., Gakwaya, A., 2002. Modeling of the metal powder compaction process using the cap model. Part I. Experimental material characterization and validation. International Journal of Solids and Structures 39 (4), 1059–1075.

Coube, O., Riedel, H., 2000. Numerical simulation of metal powder die compaction with special consideration of cracking. Powder Metallurgy 43 (2), 123–131.

Cunningham, J.C., Sinka, I.C., Zavaliangos, A., 2004. Analysis of tablet compaction. I. Characterization of mechanical behavior of powder and powder/tooling friction. Journal of Pharmaceutical Sciences 93 (8), 2022–2039.

DiMaggio, F.L., Sandler, I.S., 1971. Material model for granular soils. Journal of the Engineering Mechanics Division, American Society of Civil Engineering 97, 935–950.

Doelker, E., Massuelle, D., 2004. Benefits of die-wall instrumentation for research and development in tabletting. European Journal of Pharmaceutics and Biopharmaceutics 58, 427–444.

Drucker, D.C., Gibson, R.E., Henkel, D.J., 1957. Soil mechanics and work-hardening theories of plasticity. Transactions American Society of Civil Engineers 122, 338–346.

Eiliazadeh, B., Briscoe, B.J., Sheng, Y., Pitt, K., 2003. Investigating density distributions for tablets of different geometry during the compaction of pharmaceuticals. Particulate Science and Technology 21 (4), 303–316.

Fleck, N.A., 1995. On the cold compaction of powders. Journal of the Mechanics and Physics of Solids 43 (9), 1409–1431.

Fleck, N.A., Kuhn, L.T., McMeeking, R.M., 1992. Yielding of metal powder bonded by isolated contacts. Journal of the Mechanics and Physics of Solids 40 (5), 1139–1162.

Frenning, G., 2007. Analysis of pharmaceutical powder compaction using multiplicative hyperelasto-plastic theory. Powder Technology 172 (2), 103–112.

Helle, A.S., Easterling, K.E., Ashby, M.F., 1985. Hot-isostatic pressing diagrams: new developments. Acta Metallurgica 33 (12), 2163–2174.

Jonsén, P., Häggblad, H.-Å., 2005. Modelling and numerical investigation of the residual stress state in a green metal powder body. Powder Technology 155 (3), 196–208.

Khoei, A.R., Azizi, S., 2005. Numerical simulation of 3D powder compaction processes using cone-cap plasticity theory. Materials and Design 26, 137–147.

Long, W.M., 1960. The displacement of gas from powders during compaction. Powder Metallurgy 6, 52–72.

Martin, C.L., Bouvard, D., Shima, S., 2003. Study of particle rearrangement during powder compaction by the discrete element method. Journal of the Mechanics and Physics of Solids 51, 667–693.

Michrafy, A., Dodds, J.A., Kadiri, M.S., 2004. Wall friction in the compaction of pharmaceutical powders: measurement and effect on the density distribution. Powder Technology 148 (1), 53–55.

Michrafy, A., Ringenbacher, D., Tchoreloff, P., 2002. Modelling the compaction behaviour of powders: application to pharmaceutical powders. Powder Technology 127 (3), 257–266.

Nedderman, R.M., 1992. Statics and Kinematics of Granular Materials. Cambridge University Press, New York.

Pavier, E., Doremus, P., 1999. Triaxial characterisation of iron powder behaviour. Powder Metallurgy 42 (4), 345–352.

PM-Modnet-Modelling-Group, 1999. Comparison of computer models representing powder compaction process: state of the art review. Powder Metallurgy 42 (4), 301–311.

Procopio, A.T., Zavaliangos, A., Cunningham, J.C., 2003. Analysis of the diametrical compression test and the applicability to plastically deforming materials. Journal of Materials Science 38, 3629–3639.

Rottmann, G., Coube, O., Riedel, H., 2001. Comparison between triaxial results and models prediction with special consideration of the anisotropy. In: European Congress on Powder Metallurgy, Shrewsbury, UK, pp. 29–37.

Sandler, I.S., 2002. Review of the development of cap models for geomaterials. In: 15th ASCE Engineering Mechanics Conference, Columbia University, New York.

Sandler, I.S., DiMaggio, F.L., Baladi, G.Y., 1976. Generalized cap model for geological materials. Journal of the Geotechnical Engineering Division—ASCE 102 (7), 683–699.

Schofield, A., Wroth, C.P., 1968. Critical State Soil Mechanics. McGraw Hill, London.

Shima, S., Oyane, M., 1976. Plasticity theory for porous metals. International Journal of Mechanical Sciences 18 (6), 285–291.

Sinka, I.C., Cunningham, J.C., Zavaliangos, A., 2003. The effect of wall friction in the compaction of pharmaceutical tablets with curved faces: a validation study of the Drucker-Prager cap model. Powder Technology 133 (1–3), 33–43.

Sinka, I.C., Cunningham, J.C., Zavaliangos, A., 2004. Analysis of tablet compaction. II. Finite element analysis of density distributions in convex tablets. Journal of Pharmaceutical Sciences 93 (8), 2040–2053.

Train, D., 1957. Transmission of forces through a powder mass during the process of pelleting. Transactions of the Institution of Chemical Engineers, 266–358.

Wu, C.Y., Ruddy, O.M., Bentham, A.C., Hancock, B.C., Best, S.M., Elliott, J.A., 2005. Modelling the mechanical behaviour of pharmaceutical powders during compaction. Powder Technology 152 (1–3), 107–117.

Wu, C.Y., Hancock, B.C., Mills, A., Bentham, A.C., Best, S.M., Elliott, J.A., 2008. Numerical and experimental investigation of capping mechanisms during pharmaceutical tablet compaction. Powder Technology 181, 121–129.